

Topological laser on square lattice with gain-loss-induced higher-order corner modes

Ming-Jie Liao(廖明杰), Mei-Song Wei(韦梅松), Shuailing Wang(王帅领), Jingping Xu(许静平), Yaping Yang(羊亚平)

Citation: Chin. Phys. B, 2024, 33 (**6**): 060305. DOI: 10.1088/1674-1056/ad322a
Journal homepage: http://cpb.iphy.ac.cn; http://iopscience.iop.org/cpb

What follows is a list of articles you may be interested in

Quantum geometric tensor and the topological characterization of the extended Su-Schrieffer-Heeger model

Xiang-Long Zeng(曾相龙), Wen-Xi Lai(赖文喜), Yi-Wen Wei(魏祎雯), and Yu-Quan Ma(马余全)
Chin. Phys. B, 2024, 33 (**3**): 030310. DOI: 10.1088/1674-1056/ad1170

Observation of flat-band localized state in a one-dimensional diamond momentum lattice of ultracold atoms

Chao Zeng(曾超), Yue-Ran Shi(石悦然), Yi-Yi Mao(毛一屹), Fei-Fei Wu(武菲菲), Yan-Jun Xie(谢岩骏), Tao Yuan(苑涛), Han-Ning Dai(戴汉宁), and Yu-Ao Chen(陈宇翱)
Chin. Phys. B, 2024, 33 (**1**): 010303. DOI: 10.1088/1674-1056/ad0cd1

Progress and realization platforms of dynamic topological photonics

Qiu-Chen Yan(闫秋辰), Rui Ma(马睿), Xiao-Yong Hu(胡小永), and Qi-Huang Gong(龚旗煌)
Chin. Phys. B, 2024, 33 (**1**): 010301. DOI: 10.1088/1674-1056/acf284

Floquet dynamical quantum phase transitions in transverse *XY* spin chains under periodic kickings

Li-Na Luan(栾丽娜), Mei-Yu Zhang(张镁玉), and Lin-Cheng Wang(王林成)
Chin. Phys. B, 2023, 32 (**9**): 090302. DOI: 10.1088/1674-1056/accf68

Exact solution of slow quench dynamics and nonadiabatic characterization of topological phases

Rui Wu(邬睿), Panpan Fang(房盼攀), Chen Sun(孙辰), and Fuxiang Li(李福祥)
Chin. Phys. B, 2023, 32 (**8**): 080304. DOI: 10.1088/1674-1056/acd0a5

Topological laser on square lattice with gain–loss-induced higher-order corner modes

Ming-Jie Liao(廖明杰), Mei-Song Wei(韦梅松), Shuailing Wang(王帅领),
Jingping Xu(许静平)†, and Yaping Yang(羊亚平)‡

MOE Key Laboratory of Advanced Micro-Structured Materials, School of Physics Science and Engineering, Tongji University, Shanghai 200092, *China*

(Received 26 December 2023; revised manuscript received 26 February 2024; accepted manuscript online 11 March 2024)

We investigate the higher-order topological laser in the two-dimensional (2D) coupled-cavity array. By adding staggered on-site gain and loss to the 2D Hermitian array with a trivial phase, the system will emerge degenerate topological corner modes, which are protected by bulk band gap. For such a non-Hermitian model, by adjusting the parameters of the system and introducing the pumping into the cavity at the corner, a single-mode lasing with topological protection emerges. Furthermore, single-mode lasing exists over a wide range of pumping strengths. No matter where the cavity is initially stimulated, after enough time evolution, all the cavities belonging to the topological corner mode can emit a stable laser.

Keywords: topological corner modes, nonlinear saturated gain, single-mode lasing

PACS: 03.65.Vf, 03.65.Vf, 42.60.By, 42.60.–v **DOI:** 10.1088/1674-1056/ad322a

1. Introduction

Topological physics, as one of the important concepts of fundamental physics,[1] has been fully developed in photon,[2–14] phonon,[15–25] circuit,[26–35] and other systems in recent years. Topological photonics is one of the ideal systems for studying topological physics. For example, Liu *et al.* theoretically analyzed and experimentally verified the higher-order topological quasicrystalline insulators in photonic systems,[36] Li *et al.* utilized supersymmetric route to generate an exact topological zero mode in a 1D waveguide structure through an adiabatic evolution process,[37] Andrea *et al.* observed topological physics for various topological models by utilizing the same reprogrammable photonics platform,[38] and there have been many other studies published.[39–41] Benefiting from the introduction of non-Hermitian and nonlinear, topological photonics has been widely studied both experimentally and theoretically. One of the most successful applications of topological physics is the topological laser, which has strong robustness to the disorder and defects generated during operation. On the other hand, for the topologically protected state, such as a d-dimensional system with $(d-1)$-dimensional topological edge state, its energy level lies within the bulk band gap. As an extension of traditional topological edge states, higher-order topological systems have lower-dimensional edge states. For example, the 2D breathing kagome lattice has zero-energy states localized at three corners,[42–45] and the 2D extended Su–Schrieffer–Heeger (SSH) model has 0D corner states,[46–50] which are called second-order topological insulators and beyond the traditional bulk–edge correspondence.

The topological laser is an application in topological physics, which means that the mode of laser emission is protected by the topological system.[51–61] In recent years, for topological laser, the use of topological edge states for laser manipulation was first proposed and experimentally proved in 1D SSH models. However, due to structural limitations, it is not conducive to the realization of high-power and large-scale lasers. On the other hand, for conventional lasers, a single-mode lasing is generated near the threshold. However, the increase in pump strength will lead to the emergence of multi-mode laser, which is not conducive to the stable output of laser. In fact, topological laser based on coupled-cavity arrays can achieve fascinating results. In Ref. [52], the research is based on the Haldane-type coupled resonator array structure, which can make the system in topological edge mode by introducing on-site gain and loss. In this case, the topological laser mode propagates unidirectionally along the boundary and is protected by the topological system during transmission. Under the topological nontrivial phases, a single-mode lasing can be maintained even if the gain level is 10 times the laser threshold. A topological insulator laser was experimentally demonstrated in Ref. [53]. In that 2D topological cavity array, topological laser, which was immune to defects and distributed at the boundary of the system, was observed for the first time. Moreover, the contribution of higher-order corner state to topological lasers has also attracted attention. In the breathing kagome lattice, Ezawa theoretically analyzed the stable corner state laser by combining nonlinear and non-Hermitian.[59] Zhang *et al.* studied topological laser with low threshold in the kagome waveguide array.[58]

†Corresponding author. E-mail: xx_jj_pp@tongji.edu.cn
‡Corresponding author. E-mail: yang_yaping@tongji.edu.cn

© 2024 Chinese Physical Society and IOP Publishing Ltd

Xiong *et al.* experimentally achieved polariton corner state lasers at room temperature based on a two-dimensional extended SSH model.[62] Besides topological edge state and corner state lasers, topological bulk lasers have also been proposed. By designing topological band inversion, a bulk laser operating at room temperature can be constructed.[56,63]

In this paper, based on a 2D coupled-cavity array, we induce higher-order topological corner modes by adding on-site gain and loss to a trivial system. By adding saturated gain to the cavity at the corner of the model, we find that the eigenvalues of the other modes are almost constant except for the topological corner modes. When the pump is increased to the laser threshold, a single-mode lasing with topological protection is generated. Unlike conventional optical cavities, for this system, the topological single-mode lasing can be maintained even if the pumping strength is increased above the threshold level. Moreover, we also show the evolution of a topological laser system in the time domain, stimulating the cavity at any location, after a sufficiently long time, showing stable laser emission in the corner cavity. In fact, topological laser based on the second-order corner state has been studied in 2D SSH model,[49,50] in which the eigenvalues of corner states are mixed with these of many bulk states. The corner states are difficult to be distinguished unless more complex coupling is introduced. However, by introducing gain–loss and magnetic flux into the 2D array, the bulk gap of our proposed structure opens, making the eigenvalue of the topological corner states significantly different from these of bulk states.

The structure of this paper is as follows: in Section 2, we briefly introduce the non-Hermition coupled-cavity array model. The energy spectrum diagram and eigenmode distribution are analyzed. With on-site gain and loss, topological corner modes emerge. In Section 3, a 2D topological laser array with corner mode is explored. The dynamic evolution of the laser system is shown. In Section 4, we present a brief conclusion.

2. Non-Hermition coupled-cavity array model with on-site gain–loss

We select a 2D non-Hermitian coupled-cavity array model, as shown in Fig. 1, and this 2D model is easy to implement experimentally.[64,65] Here, the effective magnetic flux is considered to be $\phi = \pi$ for each square, which results in a phase factor $e^{i\phi}$ on the dotted lines. When the on-site gain (loss) is non-zero, the system is non-Hermitian. Obviously, in Fig. 1, the 16 orbitals (dotted box) we selected can be viewed as a unit cell, and in the experiment, the coupling between the cavity and particle gain (loss) of the cavity can be controlled independently.

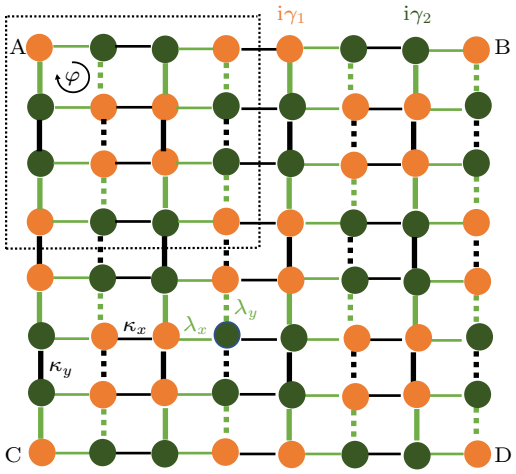


Fig. 1. Schematic of a 2D tight-binding model made by coupled-cavity array. All sites in orange (green) have on-site gain (loss) with $i\gamma$. There is the magnetic flux ϕ for each unit cell, which appears to be a tunneling phase factor $e^{i\phi}$ on the dotted lines. Here $\kappa_{x,y}$ ($\lambda_{x,y}$) represent the tunneling between different color (same) cavities along the horizontal and vertical directions, respectively.

The Hamiltonian in the momentum space is defined as[66,67]

$$H(k) = \begin{pmatrix} H_{11}(k) & H_{12}(k) & H_{13}(k) & 0 \\ H_{21}(k) & H_{22}(k) & 0 & H_{24}(k) \\ H_{31}(k) & 0 & H_{33}(k) & H_{34}(k) \\ 0 & H_{42}(k) & H_{43}(k) & H_{44}(k) \end{pmatrix}, \tag{1}$$

with

$$H_{11}(k) = H_{44}(k) = \begin{pmatrix} i\gamma_1 & \lambda_x & \lambda_y & 0 \\ \lambda_x & i\gamma_2 & 0 & e^{i\phi}\lambda_y \\ \lambda_y & 0 & i\gamma_2 & \lambda_x \\ 0 & e^{i\phi}\lambda_y & \lambda_x & i\gamma_1 \end{pmatrix},$$

$$H_{22}(k) = H_{33}(k) = \begin{pmatrix} i\gamma_2 & \lambda_x & \lambda_y & 0 \\ \lambda_x & i\gamma_1 & 0 & e^{i\phi}\lambda_y \\ \lambda_y & 0 & i\gamma_1 & \lambda_x \\ 0 & e^{i\phi}\lambda_y & \lambda_x & i\gamma_2 \end{pmatrix}, \tag{2}$$

$$H_{12}(k) = H_{21}^*(k) = \begin{pmatrix} 0 & \kappa_x e^{ik_x} & 0 & 0 \\ \kappa_x & 0 & 0 & 0 \\ 0 & 0 & 0 & \kappa_x e^{ik_x} \\ 0 & 0 & \kappa_x & 0 \end{pmatrix},$$

$$H_{13}(k) = H_{31}^*(k) = \begin{pmatrix} 0 & 0 & \kappa_y e^{ik_y} & 0 \\ 0 & 0 & 0 & \kappa_y e^{i\phi} e^{ik_y} \\ \kappa_y & 0 & 0 & 0 \\ 0 & \kappa_y e^{ik_y} & 0 & 0 \end{pmatrix}, \tag{3}$$

$$H_{24}(k) = H_{42}^*(k) = \begin{pmatrix} 0 & 0 & \kappa_x e^{ik_x} & 0 \\ 0 & 0 & 0 & \kappa_y e^{i\phi} e^{ik_y} \\ \kappa_y & 0 & 0 & 0 \\ 0 & \kappa_y e^{i\phi} & 0 & 0 \end{pmatrix},$$

$$H_{34}(k) = H_{43}^*(k) = \begin{pmatrix} 0 & \kappa_x e^{ik_x} & 0 & 0 \\ \kappa_x & 0 & 0 & 0 \\ 0 & 0 & 0 & \kappa_x e^{ik_x} \\ 0 & 0 & \kappa_x & 0 \end{pmatrix}. \tag{4}$$

Here, κ_x and κ_y represent couplings between cavities of the same color along the horizontal and vertical directions, respectively. Similarly, $\lambda_{x,y}$ are the nearest-neighbor couplings

between cavities of the different colors. In this paper, for convenience, we select $\lambda_x = \lambda_y \equiv \lambda$, $\phi = \pi$. The Hamiltonian $H(k)$ satisfies $-\Gamma H(k)^{\dagger}\Gamma = H(k)$ with $\Gamma = \sigma_x^z\sigma_y^z\tau_x^z\tau_y^z$, σ^z is the Pauli matrice, which is a pseudo-anti-Hermiticity and ensures a nontrivial topology phase with pair eigenvalues $E(k) = -E^*(k)$. Moreover, topological corner modes are characterized by the winding number, which is evaluated on the biorthogonal basis.[67–69]

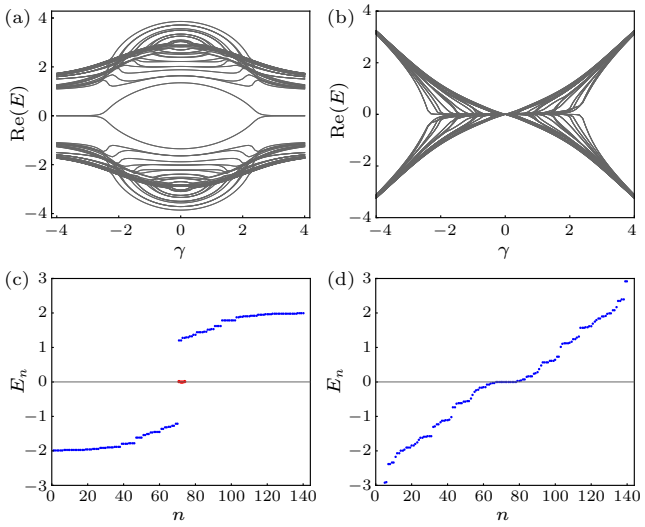


Fig. 2. Energy spectrum of the 2D non-Hermitian model composed of optical coupled-cavity array. (a) Real and (b) imaginary parts of the energy with $\phi = \pi$. Eigenvalues of the 2D non-Hermition model (c) with magnetic flux $\phi = \pi$ and (d) with magnetic flux $\phi = 0$. The common parameters in (c) and (d) are set as $\lambda = 1.8$, $\kappa_x = \kappa_y = 1$, $\gamma = 3$, and model size $L = 3$ (unit cells).

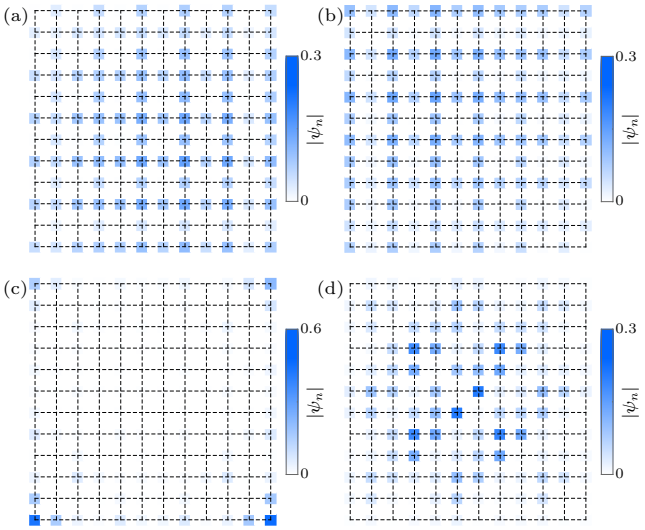


Fig. 3. The density distribution of an arbitrarily selected eigenstate, by taking $\gamma = 0$ in (a) and $\gamma = 1$ in panel (b). (c) The distribution of the topological corner mode localized at the corner cavities. (d) The distribution of a bulk mode by taking $\gamma_1 = -\gamma_2 = 3$ in panels (c) and (d). The other common parameters are same as those in Fig. 2.

In order to further understand this model, subsequently we display the distribution of the energy spectrum under open boundary conditions. Figures 2(a) and 2(b) show the real and imaginary parts of the eigenenergy with respect to γ, respectively. As $|\gamma|$ increases or decreases, the bulk gap opens or closes. Firstly, when we think about the system under the Hermitian conditions, i.e., $\gamma = 0$. Based on Fig. 2, we can see that all eigenvalues are real numbers and their imaginary parts are zero. Through the analysis of the system eigenstates under this parameter, we find that the system does not have localized states, and the system is in a metal phase or a trivial phase.[70] Figure 2(c) shows the eigenvalues of the 2D finite lattice with $\phi = \pi$. It is obvious that topological corner modes marked in red are located in bulk gap and can be found easily. Differently, Fig. 2(d) demonstrates that the energy spectrum is almost continuous and has no corner mode with $\phi = 0$. Moreover, introducing an effective magnetic flux can open the bulk gap and form topological corner mode.

Meanwhile, Fig. 3(a) displays the density distribution of an eigenstate, which is dispersed throughout the system. Subsequently, we increase γ to 1, and just like in the Hermitian case, no localized state appears, as seen in Fig. 3(b). Now, we increase γ to 3, which is greater than the critical value γ_c for the band gap closed. Figure 3(c) shows the distribution of a zero-energy mode, which is mainly localized in the four cavities around the corner. In this case, the density distribution of an arbitrarily selected bulk mode is displayed in Fig. 3(d), which is notably distributed inside the structure. Namely, the topological corner modes can be induced by introducing on-site gain–loss and an effective magnetic flux in this 2D model.

3. Two-dimensional topological laser array with corner state

Here, we investigate the dynamical evolution of the 2D laser system made of a coupled-cavity array, which is governed by a group of equations[52,53,59,69,71]

$$\mathrm{i}\frac{\mathrm{d}\psi_n}{\mathrm{d}t} = \sum_{nm} H_{nm}\psi_m + (\mathrm{i}\gamma_n + P_n)\psi_n, \tag{5}$$

where ψ_n is the amplitudes of n-th cavity with the system, and $n = 1, 2, \ldots, N$ in this model made up of N cavities. H_{nm} represents the coupling of the 2D topological array in the real space without on-site potential. P_n stands for optical saturated gain, which is obtained by stimulated emission,

$$P_n = \delta_{n,n'}\left(\frac{\mathrm{i}\gamma\xi}{1 + |\psi_n|^2/\eta}\right). \tag{6}$$

Here $\gamma\xi$ describes the amplitude of the gain and η indicates the nonlinearity of this system. When the nonlinear parameter $\eta \to \infty$, the system becomes of a linear model. Moreover, n' represents the corner sites. In other words, Eq. (6) indicates that the optical saturated gain is added only at the corner cavities of the 2D array.

In order to conform to the universal phenomenon of mode loss in optical devices, we assume that every cavity experiences loss with a rate γ_{loss}. Obviously, an unbalanced loss

system is equivalent to a gain–loss system, and it is easier to realize experimentally. Then, we introduce $\gamma_1' = \gamma_1 - \gamma_{\text{loss}}$ and $\gamma_2' = \gamma_2 - \gamma_{\text{loss}}$ for all red and blue sites.

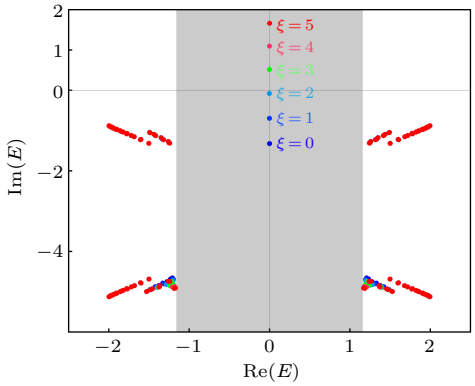


Fig. 4. Real and imaginary parts of the spectrum with the increase pump strength ξ in the linear limit $\eta \to \infty$. We have set $\lambda = 1.8$, $\kappa_x = \kappa_y = 1$, $\gamma = 0.5$, $\gamma_{\text{loss}} = 3$, and $\phi = \pi$.

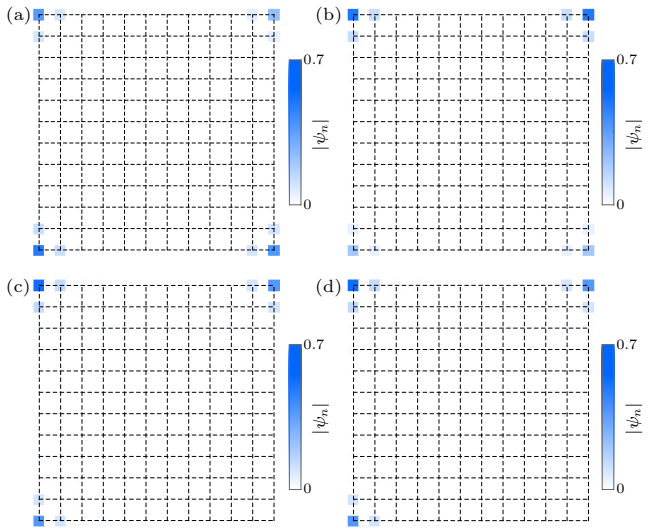


Fig. 5. The density distribution of four degenerate topological corner modes with $\xi = 4$. The other common parameters are same as those in Fig. 4.

Now, we first show the energy spectrum of the 2D non-Hermitian system in the linear limit with $\eta \to \infty$. Figure 4 denotes the changes of the real and imaginary parts of the spectrum at different ξ. We can see that the topological corner modes always exist in the bulk band gap. However, when ξ is not large enough, the eigenvalue corresponding to the topological corner mode has a negative imaginary part, so that the topological corner mode cannot be excited effectively. Clearly, Fig. 4 shows that the laser threshold ξ_{thr} for the topological corner mode is slightly greater than 2. When $\xi < \xi_{\text{thr}}$, Im(E) of the corner mode is negative within the band gap, and all eigenstates are lossy modes. However, for $\xi > \xi_{\text{thr}}$, only the Im(E) of the corner modes change from negative to positive, whereas the Im(E) of the bulk modes changes very slightly. In other words, except for the topological corner mode, all the other modes in the system are loss modes. With increasing ξ, the imaginary part of the corner modes changes significantly. Obviously, this facilitates the construction of single-mode lasing based on topological corner mode with a wide range of the pump strength ξ. Figure 5 displays the density profile of the degenerate topological corner modes. It shows that the energy is mainly distributed in the four corner cavities of the 2D system.

Then, we consider the nonlinear dynamics with $\eta = 1$ of the 2D laser system. In order to analyze the stability of a laser system, it is necessary to analyze it in the time domain. The dynamic evolution of the laser system is described by the Schrödinger equation. Figure 6(a) displays the time evolution of four corner sites of this 2D tight-binding model, which are marked as A, B, C, and D. Initially, cavity A is stimulated and quickly reaches saturated amplitude. The amplitudes of cavities B and C, which are equidistant from cavity A, are highly synchronized over time. When $t = 23$, the amplitudes of $|\psi_{\text{B}}|$ and $|\psi_{\text{C}}|$ reach saturation and are same as cavity A. However, for cavity D, it takes longer to reach saturated amplitude and is eventually equal to the other three cavities. On the other hand, we should examine the field density distribution of the system in a steady state. As an example, Fig. 6(b) shows the density distribution of the steady state with $\xi = 3$. One can observe that the density distribution is homogeneously distributed on the four cavities around the corner, similar to the eigenfield shown in Fig. 5(a). Therefore, after a long enough time, the system reaches a steady state and is in the single-mode region. Clearly, it indicates that the single-mode lasing can be constructed based on the topological corner modes of this 2D model.

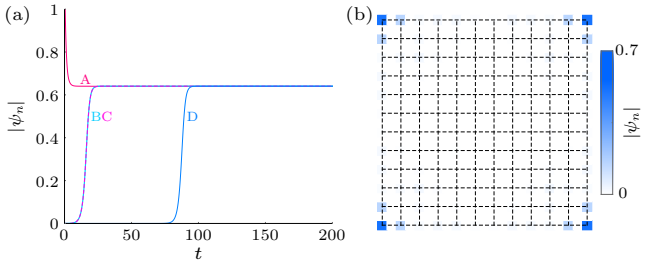


Fig. 6. (a) Amplitudes $|\psi_n|$ for different cavities as a function of t in this system. (b) Density distribution of the steady state after a long-time evolution. Here we have set $L = 3$, $\xi = 3$, $\lambda = 1.8$, $\kappa_x = \kappa_y = 1$, $\gamma = 0.5$, $\gamma_{\text{loss}} = 3$, and $\eta = 1$.

Here, we also show the dynamical evolution of the system under different initial conditions, as seen in Fig. 7. Figures 7(a1)–7(a4) show the evolution of the whole system when a corner cavity was initially stimulated. Clearly, cavities B and C evolve synchronously. About $t = 100$, the four corner cavities reach the equal saturated amplitude, consistent with Fig. 6(a). For the case that the edge cavity was stimulated initially, cavity A closest to it can get energy fastest, while cavities B and D require longer time to obtain energy, as seen in Figs. 7(b1)–7(b4). Correspondingly, the evolutions of amplitude ψ_n in cavities A, B, C, and D are displayed in Fig. 8(a),

which reveals that those corner cavities take different times to reach the same saturated amplitude. Figures 7(c1)–7(c4) indicate that cavities B, C, and D evolve synchronously and reach the same steady amplitude. However, cavity A takes longer to reach its maximum amplitude. The time for the corner cavity to reach saturated amplitude is related to the distance from the cavity stimulated initially. For the bulk cavity, due to the complexity of the propagation path, the nearest cavity A is the slowest to reach saturated amplitude. On the other hand, the energy tends to transfer in the direction of the gain cavity. In Fig. 7(c), the right side of the initial stimulated cavity is a gain cavity, and the left side is a loss cavity. Thus, the energy tends to flow in the direction to cavity D, and cavity A reaches the steady state later. In Fig. 7(d), the left of the initial stimulated cavity is a gain cavity, while the right one is a loss cavity. The results in Fig. 7(d) are different from those in Fig. 7(c), where cavity A reaches the steady amplitudes earlier than cavity D. According to Figs. 7 and 8, it can be seen that regardless of the initial conditions, the field density distribution finally concentrates in cavities A, B, C, and D with the same saturated amplitude.

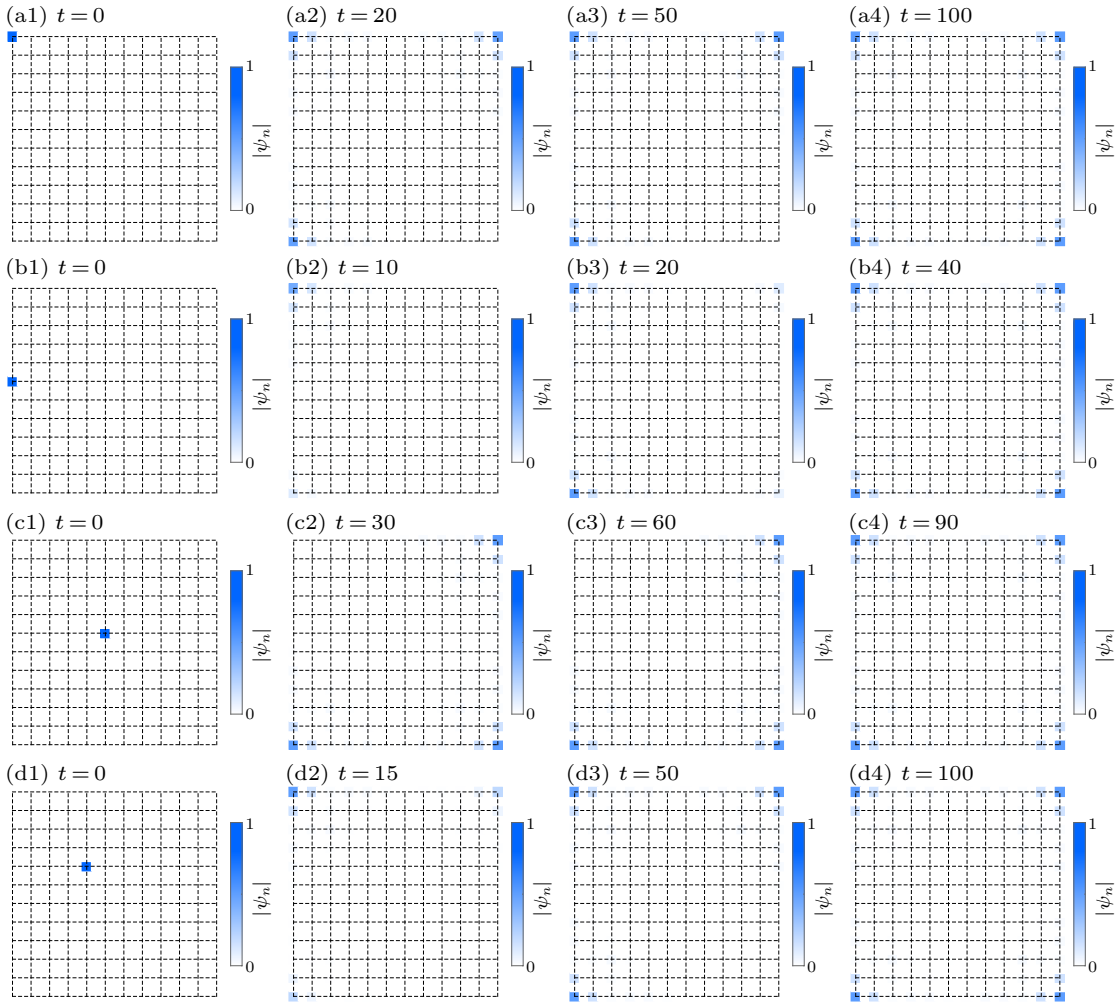


Fig. 7. Time evolution of the whole system with initially stimulated (a1)–(a4) corner cavity, (b1)–(b4) edge cavity, (c1)–(c4) bulk cavity, and (d1)–(d4) another bulk cavity. The parameters are chosen to be $L=3$, $\lambda=1.8$, $\kappa_x=\kappa_y=1$, $\gamma=0.5$, $\phi=\pi$, and $\eta=1$.

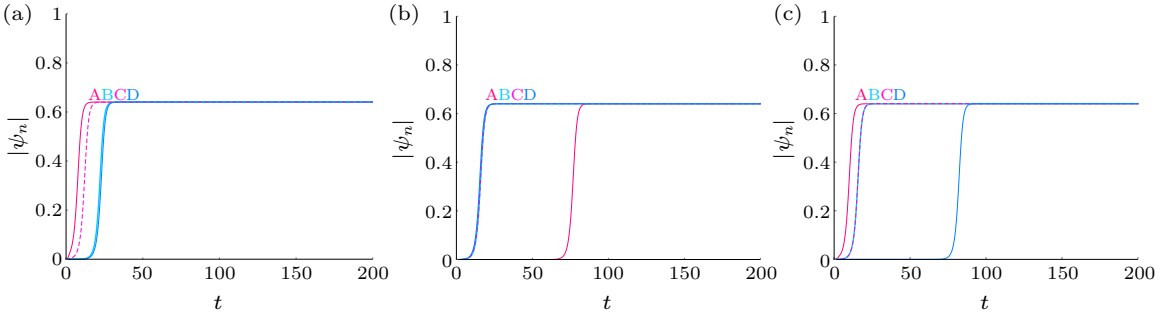


Fig. 8. Amplitudes $|\psi_n|$ for different cavities as a function of t under the initial condition (a) corresponding to Figs. 7(b1)–7(b4), (b) corresponding to Figs. 7(c1)–7(c4), and (c) corresponding to Figs. 7(d1)–7(d4).

In this section, based on the 2D non-Hermitian system, we clearly show that in the linear limit with $\eta \to \infty$, only the topological corner modes change significantly when the pump strength ξ is increased, and the single-mode lasing can still be maintained when the pump strength is greater than the laser threshold. Subsequently, we combine the nonlinear with non-Hermitian, and one can notice that no matter which cavity of the system is excited at the initial moment, after enough time, all the cavities of the corner state can output the laser stably.

4. Conclusions

In summary, we consider a 2D array with higher-order topological corner modes that can be introduced by adding staggered gain–loss and magnetic flux to this system. We leave the system at a unbalanced global loss and add the saturated gain to a few specific cavities. It is found that only the eigenvalue Im(E) of the topological corner modes changes from negative to positive, in which the laser threshold is easily found. When we stimulate any cavity, the cavities belonging to the topological corner modes have the same saturated amplitude when they reach the steady state. We also show the dynamic emission of the laser in real space. Here, we show that a high-power laser can be manufactured with topological properties, namely, a single-mode lasing that can be maintained when the pumping coefficient is much higher than the laser threshold. We hope this work can enrich nonlinear non-Hermitian higher-order topological single-mode lasing.

Acknowledgments

This work was supported by the National Natural Science Foundation of China (Grant Nos. 12274326 and 12174288) and the National Key R&D Program of China (Grant No. 2021YFA1400602).

References

[1] Qi X L and Zhang S C 2011 *Rev. Mod. Phys.* **83** 1057
[2] Haldane F D M and Raghu S 2008 *Phys. Rev. Lett.* **100** 013904
[3] Raghu S and Haldane F D M 2008 *Phys. Rev. A* **78** 033834
[4] Khanikaev A B, Mousavi S H, Tse W K, Kargarian M, MacDonald A H and Shvets G 2013 *Nat. Mater.* **12** 233
[5] Hafezi M, Mittal S, Fan J, Migdall A and Taylor J M 2013 *Nat. Photon.* **7** 1001
[6] Rechtsman M C, Zeuner J M, Plotnik Y, Lumer Y, Podolsky D, Dreisow F, Nolte S, Segev M and Szameit A 2013 *Nature* **496** 196
[7] Wu L H and Hu X 2015 *Phys. Rev. Lett.* **114** 223901
[8] Leykam D and Chong Y D 2016 *Phys. Rev. Lett.* **117** 143901
[9] Slobozhanyuk A P, Khanikaev A B, Filonov D S, Smirnova D A, Miroshnichenko A E and Kivshar Y S 2016 *Sci. Rep.* **6** 22270
[10] Khanikaev A B and Shvets G 2017 *Nat. Photon.* **11** 763
[11] Ota Y, Katsumi R, Watanabe K, Iwamoto S and Arakawa Y 2018 *Commun. Phys.* **1** 86
[12] Ota Y, Liu F, Katsumi R, Watanabe K, Wakabayashi K, Arakawa Y and Iwamoto S 2019 *Optica* **6** 786
[13] Hassan A E, Kunst F K, Moritz A, Andler G, Bergholtz E J and Bourennane M 2019 *Nat. Photon.* **13** 697
[14] Yoshimi H, Yamaguchi T, Ota Y, Arakawa Y and Iwamoto S 2020 *Opt. Lett.* **45** 2648
[15] Prodan E and Prodan C 2009 *Phys. Rev. Lett.* **103** 248101
[16] Yang Z J, Gao F, Shi X H, Lin X, Gao Z, Chong Y Y and Zhang B L 2015 *Phys. Rev. Lett.* **114** 114301
[17] Stenull O, Kane C L and Lubensky T C 2016 *Phys. Rev. Lett.* **117** 068001
[18] Liu Y Z, Xu Y, Zhang S C and Duan W H 2017 *Phys. Rev. B* **96** 064106
[19] Singh S, Wu Q S, Yue C M, Romero A H and Soluyanov A A 2018 *Phys. Rev. Mater.* **2** 114204
[20] Saha K and Garate I 2014 *Phys. Rev. B* **89** 205103
[21] Li J X, Wang L, Liu J X, Li R H, Zhang Z Y and Chen X Q 2020 *Phys. Rev. B* **101** 081403
[22] Ren H J, Shah T, Pfeifer H, Brendel C, Peano V, Marquardt F and Painter O 2022 *Nat. Commun.* **13** 3476
[23] Liu Y Z, Zou N L, Zhao S B, Chen X B, Xu Y and Duan W H 2022 *Nano Lett.* **22** 2120
[24] Yang Y, Wang J H, Liu Y, Cui Y T, Ding G Q and Wang X T 2023 *Phys. Rev. B* **107** 024304
[25] Amigo M G, Vergniory M G, Errea I and Manes J L 2023 *Phys. Rev. B* **107** 144307
[26] Ningyuan J, Owens C, Sommer A, Schuster D and Simon J 2015 *Phys. Rev. X* **5** 021031
[27] Albert V V, Glazman L I and Jiang L 2015 *Phys. Rev. Lett.* **114** 173902
[28] Hadad Y, Soric J C, Khanikaev A B and Alù A 2018 *Nat. Electron.* **1** 178
[29] Zhao E 2018 *Ann Phys.* **399** 289
[30] Lee C H, Imhof S, Berger C, Bayer F, Brehm J, Molenkamp L W, Kiessling T and Thomale R 2018 *Commun. Phys.* **1** 39
[31] Imhof S, Berger C, Bayer F, Brehm J, Molenkamp L W, Kiessling T, Schindler F, Lee C H, Greiter M, Neupert T and Thomale R 2018 *Nat. Phys.* **14** 925
[32] Liu S, Ma S J, Zhang Q, Zhang L, Yang C H, You O, Gao W L, Xiang J Y, Cui T J and Zhang S 2020 *Light Sci. Appl.* **9** 145
[33] Wang Y, Price H M, Zhang B L and Chong Y D 2020 *Nat. Commun.* **22** 2356
[34] Olekhno N A, Kretov E I, Stepanenko A A, Ivanova P A, Yaroshenko V V, Puhtina E M, Filonov D S, Cappello B, Matekovits L and Gorlach M A 2022 *Nat. Commun.* **11** 1436
[35] Zou D Y, Chen T, He W J, Bao J C, Lee CH H, Sun H J and Zhang X D 2021 *Nat. Commun.* **12** 7201
[36] Shi A Q, Peng Y W, Jiang J P, Peng Y C, Peng P, Chen J Z, Chen H S, Wen S C, Lin X, Gao F and Liu J J 2024 *Laser Photon. Rev.* **2024** 2300956
[37] Liu X Y, Lin Z Y, Song W E, Sun J C, Huang C Y, Wu S J, Xiao X J, Xin H R, Zhu S N and Li T 2024 *Phys. Rev. Lett.* **132** 016601
[38] On M B, Ashtiani F, Sanchez-Jacome D, Perez-Lopez D, Yoo S J B and Blanco-Redondo A 2024 *Nat. Commun.* **15** 629
[39] Xu Q X, Peng Y C, Shi A Q, Peng P and Liu J J 2024 *J. Opt. Soc. Am. A* **41** 366
[40] Khanikaev A B and Alù A 2024 *Nat. Commun.* **15** 931
[41] Fritzsche A, Biesenthal T, Maczewsky L J, Becker K, Ehrhardt M, Heinrich M, Thomale R, Joglekar Y N and Szameit A 2024 *Nat. Mater.* **23** 377
[42] Guo H M and Franz M 2009 *Phys. Rev. B* **80** 113102
[43] Xue H Y, Yang Y H, Gao F, Chong Y D and Zhang B L 2019 *Nat. Mater.* **18** 108
[44] Lu X C, Chen Y and Chen H Y 2020 *Phys. Rev. B* **101** 195143
[45] Shen K, Deng W M, Mo H C, Shi F L, Ma F, Chen X D and Dong J W 2023 *Opt. Lett.* **48** 2825
[46] Ma H Y, Zhang Z, Fu P H, Wu J S and Yu X L 2022 *Phys. Rev. B* **106** 245109
[47] Li C A, Choi S J, Zhang S B and Trauzettel B 2022 *Phys. Rev. Res.* **4** 023193
[48] Li S, Yan X X, Gao J H and Hu Y 2022 *Opt. Express* **30** 17054
[49] Zhang W H, Xie X, Hao H M, Dang J C, Xiao S, Shi S S, Ni H Q, Niu Z C, Wang C, Jin K J, Zhang X D, and Xu X L 2020 *Light Sci. Appl.* **9** 109
[50] Wei M S, Liao M J, Wang C, Zhu C J, Yang Y P and Xu J P 2023 *Opt. Express* **31** 3427
[51] Bahari B, Ndao A, Vallini F, Amili A E, Fainman Y and Kanté B 2017 *Science* **358** 636
[52] Harari G, Bandres M A, Lumer Y, Rechtsman M C, Chong Y D, Khajavikhan M, Christodoulides D N and Segev M 2018 *Science* **359** eaar4003

[53] Bandres M A, Wittek S, Harari G, Parto M, Ren J H, Segev M, Christodoulides D N and Khajavikhan M 2018 *Science* **359** eaar4005
[54] Zeng Y Q, Chattopadhyay U, Zhu B F, Qiang B, Li J H, Jin Y H, Li L H, Davies A G, Linfield E H, Zhang B L, Chong Y D and Wang Q J 2020 *Nature* **578** 246
[55] Amelio I and Carusotto I 2020 *Phys. Rev. X* **10** 041060
[56] Shao Z K, Chen H Z, Wang S, Mao X R, Yang Z Q, Wang S L, Wang X X, Hu X and Ma R M 2020 *Nat. Nanotechnol.* **15** 67
[57] Pelous A L, Amelio I, SecIÍ M and Carusotto I 2021 *Phys. Rev. A* **104** 053516
[58] Zhong H, Kartashov Y V, Szameit A, Li Y D, Liu C L and Zhang Y Q 2021 *APL Photon.* **6** 040802
[59] Ezawa M 2022 *Phys. Rev. Res.* **4** 013195
[60] Gong Y K, Wong S, Bennett A J, Huffaker D L and Oh S S 2022 *ACS Photon.* **7** 2089
[61] Tian J Y, Tan Q Y, Wang Y T, Yang Y H, Yuan G H, Adamo G and Soci C 2023 *Nat. Commun.* **14** 1433
[62] Wu J Q, Ghosh S J, Gan Y S, Shi Y, Mandal S, Sun H D, Zhang B L, Liew T C H, Su R and Xiong Q H 2023 *Sci. Adv.* **9** eadg4322
[63] Han S, Cui J Y, Chua Y D, Zeng Y Q, Hu L X, Dai M J, Wang F K, Sun F Y, Zhu S, Li L H, Davies A G, Linfield E H, Tan C S, Kivshar Y and Wang Q J 2023 *Light Sci. Appl.* **12** 145
[64] Longhi S, Gatti D and Valle G D 2015 *Sci. Rep.* **5** 13376
[65] Mittal S, Orre V V, Zhu G Y, Gorlach M A, Poddubny A and Hafezi M 2019 *Nat. Photon.* **13** 692
[66] Wheeler W A, Wagner L K and Hughes T L 2019 *Phys. Rev. B* **100** 245135
[67] Luo X W and Zhang C W 2019 *Phys. Rev. Lett.* **123** 073601
[68] Wei Y Z, Yan B, Peng Y C, Shi A Q, Zhao D Y, Peng R, Xiang Y J and Liu J J 2021 *Opt. Lett.* **46** 3941
[69] Zhu B F, Wang Q, Zeng Y Q, Wang Q J and Chong Y D 2021 *Phys. Rev. B* **104** L140306
[70] Benalcazar W A, Bernevig B A and Hughes T L 2017 *Phys. Rev. B* **96** 245115
[71] Zhu B F, Wang Q, Leykam D L, Xue H R, Wang Q J and Chong Y D 2022 *Phys. Rev. Lett* **129** 013903